Light trapping with plasmonic particles: beyond the dipole model

Fiona J. Beck,[1,2,*] Sudha Mokkapati,[1] and Kylie R. Catchpole[1]

[1]*Centre for Sustainable Energy Systems, College of Engineering and Computer Science, The Australian National University, Canberra, ACT 0200, Australia*
[2]*ICFO-Institut de Ciencies Fotonique, 08860 Castelldefels (Barcelona), Spain*
[*]*fiona.beck@icfo.es*

Abstract: Disk-shaped metal nanoparticles on high-index substrates can support resonant surface plasmon polariton (SPP) modes at the interface between the particle and the substrate. We demonstrate that this new conceptual model of nanoparticle scattering allows clear predictive abilities, beyond the dipole model. As would be expected from the nature of the mode, the SPP resonance is very sensitive to the area in contact with the substrate, and insensitive to particle height. We can employ this new understanding to minimise mode out-coupling and Ohmic losses in the particles. Taking into account optical losses due to parasitic absorption and outcoupling of scattered light, we estimate that an optimal array of nanoparticles on a 2 μm Si substrate can provide up to 71% of the enhancement in absorption achievable with an ideal Lambertian rear-reflector. This result compares to an estimate of 67% for conventional pyramid-type light trapping schemes.

OCIS codes: (250.5403) Plasmonics; (350.6050) Solar energy.

References and Links

1. H. A. Atwater and A. Polman, "Plasmonics for improved photovoltaic devices," Nat. Mater. **9**(3), 205–213 (2010).
2. F. J. Beck, S. Mokkapati, and K. R. Catchpole, "Plasmonic light-trapping for Si solar cells using self-assembled, Ag nanoparticles," Prog. Photovolt. Res. Appl. **18**(7), 500–504 (2010).
3. Z. Ouyang, S. Pillai, F. Beck, O. Kunz, S. Varlamov, K. R. Catchpole, P. Campbell, and M. A. Green, "Effective light trapping in polycrystalline silicon thin-film solar cells by means of rear localized surface plasmons," Appl. Phys. Lett. **96**(26), 261109 (2010).
4. S. Pillai, K. R. Catchpole, T. Trupke, and M. A. Green, "Surface plasmon enhanced silicon solar cells," J. Appl. Phys. **101**(9), 093105 (2007).
5. D. Derkacs, S. H. Lim, P. Matheu, W. Mar, and E. T. Yu, "Improved performance of amorphous silicon solar cells via scattering from surface plasmon polaritons in nearby metallic nanoparticles," Appl. Phys. Lett. **89**(9), 093103 (2006).
6. K. Nakayama, K. Tanabe, and H. A. Atwater, "Plasmonic nanoparticle enhancement light absorption in GaAs solar cells," Appl. Phys. Lett. **93**(12), 121904 (2008).
7. D. Derkacs, W. V. Chen, P. M. Matheu, S. H. Lim, P. K. L. Yu, and E. T. Yu, "Nanoparticle-induced light scattering for improved performance of quantum-well solar cells," Appl. Phys. Lett. **93**(9), 91103–91107 (2008).
8. Y. A. Akimov, W. S. Koh, and K. Ostrikov, "Enhancement of optical absorption in thin-film solar cells through the excitation of higher-order nanoparticle plasmon modes," Opt. Express **17**(12), 10195–10205 (2009).
9. B. J. Soller and D. G. Hall, "Scattering enhancement from an array of interacting dipoles near a planar waveguide," J. Opt. Soc. Am. B **19**(10), 2437–2448 (2002).
10. K. R. Catchpole and S. Pillai, "Absorption enhancement due to scattering by dipoles into silicon waveguides," J. Appl. Phys. **100**(4), 44504 (2006).
11. K. R. Catchpole and A. Polman, "Plasmonic solar cells," Opt. Express **16**(26), 21793–21800 (2008).
12. J. C. Mertz, "Radiative absorption, fluorescence, and scattering of a classical dipole near a lossless interface: a unified description," J. Opt. Soc. Am. B **17**(11), 1906 (2000).
13. K. R. Catchpole and A. Polman, "Design principles for particle plasmon enhanced solar cells," Appl. Phys. Lett. **93**(19), 191113 (2008).
14. F. J. Beck, S. Mokkapati, A. Polman, and K. R. Catchpole, "Asymmetry in photocurrent enhancement by plasmonic nanoparticle arrays located on the front or on the rear of solar cells," Appl. Phys. Lett. **96**(3), 33113 (2010).

#153057 - $15.00 USD Received 19 Aug 2011; revised 19 Sep 2011; accepted 20 Sep 2011; published 23 Nov 2011

15. C. Hägglund, M. Zäch, P. Goran, and K. Bengt, "Electromagnetic coupling of light into a silicon solar cell by nanodisk plasmons," Appl. Phys. Lett. **92**(5), 53110 (2008).
16. S. Pillai, F. J. Beck, K. R. Catchpole, Z. Ouyang, and M. A. Green, "The effect of dielectric spacer layer thickness on surface plasmon enhanced solar cells for front and rear side depositions," J. Appl. Phys. **109**(7), 073105 (2011).
17. F. J. Beck, E. Verhagen, S. Mokkapati, A. Polman, and K. R. Catchpole, "Resonant SPP modes supported by discrete metal nanoparticles on high-index substrates," Opt. Express **19**(S2), A146–A156 (2011).
18. T. L. Temple, H. S. Mahanama, H. S. Reehal, and D. M. Bagnall, "Influence of localised surface plasmon excitation in silver nanoparticles on the performance of silicon solar cells," Sol. Energy Mater. Sol. Cells **93**(11), 1978–1985 (2009).
19. P. B. Johnson and R. W. Christy, "Optical constants of the noble metals," Phys. Rev. B **6**(12), 4370–4379 (1972).
20. M. J. Keevers and M. A. Green, "Absorption edge of silicon from solar cell spectral response measurements," Appl. Phys. Lett. **66**(2), 174–176 (1995).
21. S. H. Lim, W. Mar, P. Matheu, D. Derkacs, and E. T. Yu, "Photocurrent spectroscopy of optical absorption enhancement in silicon photodiodes via scattering from surface plasmon polaritons in gold nanoparticles," J. Appl. Phys. **101**(10), 104309 (2007).
22. P. Spinelli, C. van Lare, E. Verhagen, and A. Polman, "Controlling Fano lineshapes in plasmon-mediated light coupling into a substrate," Opt. Express **19**(S3 Suppl 3), A303–A311 (2011).
23. S. Fan, W. Suh, and J. D. Joannopoulos, "Temporal coupled-mode theory for the Fano resonance in optical resonators," J. Opt. Soc. Am. A **20**(3), 569–572 (2003).
24. I. Diukman and M. Orenstein, "How front side plasmonic nanostructures enhance solar cell efficiency," Sol. Energy Mater. Sol. Cells **95**(9), 2628–2631 (2011).
25. F. J. Beck, A. Polman, and K. R. Catchpole, "Tunable light trapping for solar cells using localized surface plasmons," J. Appl. Phys. **105**(11), 114310 (2009).
26. A. Centeno, J. Breeze, B. Ahmed, H. Reehal, and N. Alford, "Scattering of light into silicon by spherical and hemispherical silver nanoparticles," Opt. Lett. **35**(1), 76–78 (2010).
27. C. Rockstuhl, S. Fahr, K. Bittkau, T. Beckers, R. Carius, F. J. Haug, T. Söderström, C. Ballif, and F. Lederer, "Comparison and optimization of randomly textured surfaces in thin-film solar cells," Opt. Express **18**(S3), A335–A341 (2010).
28. C. F. Bohren and D. R. Huffman, *Absorption and scattering of light by small particles*. (Wiley, New York: 1983).
29. A. Goetzberger, "Optical confinement in thin Si solar cells by diffuse back reflections," in 15th Photovoltaic Specialists Conference, (1981).
30. M. A. Green, "Lambertian light trapping in textured solar cells and light emitting diodes: analytical solutions," Prog. Photovolt. Res. Appl. **10**(4), 235–241 (2002).
31. S. Mokkapati, F. J. Beck, R. de Waele, A. Polman, and K. R. Catchpole, "Resonant nano-antennas for light trapping in plasmonic solar cells," J. Phys. D Appl. Phys. **44**(18), 185101 (2011).
32. P. Yeh, *Optical Waves in Layered Media* (Wiley, New York, 1998).
33. T. Trupke, E. Daub, and P. Würfel, "Absorptivity of silicon solar cells obtained from luminescence," Sol. Energy Mater. Sol. Cells **53**(1-2), 103–114 (1998).
34. P. Wurfel, *Physik der Solarzellen. Spektrum* (Akademischer Verlag GmbH, Heidelberg, Berlin, Oxford, 1995).

1. Introduction

Over the last decade, scattering from plasmonic nanostructures has been successfully employed for light trapping applications in opto-electronic devices [1]. Sub-wavelength metal particles in free space can support optically driven localised surface plasmons which can be designed to have large scattering resonances. If these particles are in the vicinity of a high refractive index substrate, light is scattered preferentially into the optically dense medium, over a wide range of angles. This can be employed to efficiently couple incident light into trapped modes in a solar cell, increasing the absorption in the active region, and hence the efficiency. To date, numerous experimental demonstrations have been published on Si [2–5] , GaAs [6], and quantum-well solar cells [7].

To achieve effective light trapping, nanoparticle arrays should be designed to be strongly scattering, with low Ohmic losses and efficient coupling to the cell. The details of the nanoparticle shape and size, and the proximity of the high-refractive index substrate determine the scattering behaviour. Initial studies have employed the dipole model to explain the trends in nanoparticle scattering [8–10] and provide criteria for designing plasmonic light trapping structures [11]. The proximity of the substrate changes the scattering behaviour by modifying the polarisability, the electric field driving the resonance, and the angular distribution of the scattered light [12]. The shape of the nanoparticle should be chosen to ensure that the effective dipole moment induced in the particle is close to the interface, in

#153057 - $15.00 USD Received 19 Aug 2011; revised 19 Sep 2011; accepted 20 Sep 2011; published 23 Nov 2011

order to achieve good in-coupling into the cell [13]. Additionally, the thickness of the dielectric spacer layer separating particles from the substrate, should be optimised for both the coupling efficiency [11], and to ensure strong scattering [14].

However, the dipole analogy breaks down when particles are very close to a high index substrate and have significant surface contact with the interface. It has been observed that within tens of nanometres from an Si substrate, nanoparticle scattering behaviour is very sensitive to changes in the spacer layer thickness [14], [15]. Additionally, anomalously high scattering cross-sections are observed for particles directly on the rear of a Si substrate [14]. This has since been experimentally verified, with larger photocurrent enhancements occurring at long wavelengths for thin, Si solar cells, sensitised with rear-located, Ag nanoparticles [3], [16].

We have recently demonstrated that different types of resonant modes can be supported by disk-shaped nanoparticles on high-index substrates [17]. At short wavelengths, a scattering resonance is observed that can be attributed to a localised surface plasmon (LSP) resonance, with the near-field of the mode localised at the top of the particle, in the air region. Conversely, at long wavelengths, the scattering resonances observed are localised at the substrate side of the nanoparticle. This mode has been attributed to geometrical resonances of surface plasmon polaritons (SPPs) at the Ag/Si interface, confined to the area of the particle. Light scattered by the particle is coupled into SPP modes at the interface, and resonances occur when the diameter of the disk is roughly equal to $^{m}/_{2}\ \lambda_{spp} + l_{\varphi}$, where λ_{spp} is the wavelength of the SPP, l_{φ} is due to the phase-shift introduced by reflection at the sides of the particle, and m is an integer. These types of resonant SPP modes are interesting for light trapping applications as they can have very high scattering cross-sections when placed directly on high-index substrates; up to 7.5 times larger than that of a dipole-like scatterer with an equivalent free space resonance [17].

In this work, we show that this new resonant SPP model provides a wide range of predictive capabilities. Since the SPP mode is localised at the interface between the particle and the substrate, we would expect it to be very sensitive to the area in contact with the substrate, and insensitive to particle height. Using numerical FDTD simulations we demonstrate that this is indeed the case. Additionally, we show that trends in the out-coupling and Ohmic losses in the particles can be qualitatively understood by invoking the resonant SPP description. Furthermore, we evaluate the potential for light trapping with plasmonic structures by employing a multiple scattering model, and discuss the relative contribution of losses due to the angular spectrum of scattered light and the out-coupling and Ohmic losses.

2. Design principles

To investigate the scattering behaviour of plasmonic nanoparticles that support resonant SPP modes on Si substrates, 3D finite-difference, time-domain (FDTD) numerical simulations were performed. A single, disk-shaped Ag particle on a semi-infinite Si substrate was modelled using the FDTD solutions package from Lumerical [18]. The simulation volume was terminated by perfectly matched layer boundary conditions. Linearly polarised radiation from the normally incident source was propagated from the air region to the substrate, corresponding to nanoparticles on the front of the Si, or from the substrate to air, corresponding to nanoparticles on the rear. For particles on the rear, the source is incident 50 nm from the Si interface, to minimise the amount of light absorbed in the Si before reaching the particle. The dielectric functions of the materials were modelled using a Drude model for Ag, fitted to optical data from Johnson and Christy [19], and a Drude-Lorentz model for Si, fitted to data from Keevers and Green [20].

The total power absorbed by the nanoparticle, P_{abs}, was calculated by integrating the Poynting vector of the total field (incident plus scattered) over a closed surface surrounding the particle. The normalised absorption cross-section is then calculated by $Q_{abs} = P_{abs}/(P_{inc}A_{xs})$, where P_{inc} is the incident source power, and A_{xs} is the cross-sectional area of the particle. Similarly, the scattered power was calculated from the integrated Poynting vector of the scattered field. This was evaluated separately in the air, $P_{scat,air,}$ and in the substrate, $P_{scat,subs}$.

#153057 - $15.00 USD Received 19 Aug 2011; revised 19 Sep 2011; accepted 20 Sep 2011; published 23 Nov 2011

In the Si the surface over which the integration is performed is 100 nm from the interface; for wavelengths above 500 nm, less than 10% of the light is absorbed in the Si before reaching the monitor. This allows the fraction of scattered light coupled into the substrate, also referred to as the coupling efficiency, to be calculated as $F_{subs} = P_{scat,subs}/(P_{scat,air} + P_{scat,subs})$. The normalised scattering cross-section, Q_{scat}, is then determined from the total scattered power in the same manner as Q_{abs}. From these cross sections we can define the scattering efficiency of the particle as $\eta_{scat} = Q_{scat}/(Q_{scat} + Q_{abs})$.

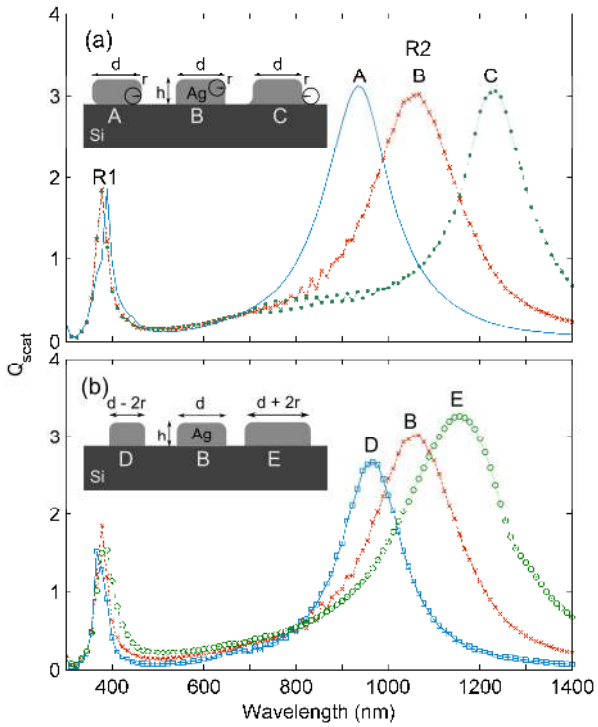

Fig. 1. Calculated normalised scattering cross-section (Q_{scat}) for Ag nanoparticles directly on a Si substrate, with light normally incident from the air. Data is shown for (a) Ag disks of height h = 50 nm and diameter d = 100 nm with rounded top edges, and bottom edges that are either rounded (particle A), straight (particle B), or splayed (particle C) with a radius of curvature, r = 10 nm, as shown in the schematic inset, and (b) for Ag disks with straight bottom edges and diameters of either d = 100 nm (particle B), d-2r = 80 nm (particle D) or d+2r = 120 nm (particle E).

2.1 Front located nanoparticles

Figure 1 shows the calculated scattering cross-section, Q_{scat}, for a single, disk-shaped particle on the front of a Si substrate, with light incident from air. Two distinct peaks in the scattering spectra are observed for all disk geometries: one at short wavelengths, R1, corresponding to a LSP localised at the top of the particle; and one at long wavelengths, R2, corresponding to a resonant SPP mode [19]. For particles on the rear of a substrate (with light incident from the Si) the same types of resonances are observed. Here, we study front-located particles, to allow comparison of the relative strengths of the modes, avoiding the absorption of incident light in the Si substrate at short wavelengths around R1.

In Fig. 1(a), spectra are shown for a single Ag disk with different edge shapes, as illustrated in the schematic. All particles have rounded top edges, and bottom edges that are either rounded (particle A), straight (particle B), or splayed (particle C), with a radius of curvature, r = 10 nm. It is clear that the R1 mode is not significantly affected by the change in the shape of the bottom edge. However, the R2 resonance wavelength is blue-shifted by $\Delta\lambda_{R2}$

#153057 - $15.00 USD Received 19 Aug 2011; revised 19 Sep 2011; accepted 20 Sep 2011; published 23 Nov 2011

= 132 nm when the edges are rounded, and red-shifted by $\Delta\lambda_{R2}$ = 157 nm when the edges are splayed. We attribute these shifts to the nature of the mode excited at R2. Since the resonant SPP occurs at the Ag/Si interface, the resonance wavelength is determined by the diameter of the area in contact substrate, rather than the diameter of the particle as a whole.

We verify this in Fig. 1(b), by plotting Q_{scat} spectra for disks that have straight bottom edges, and diameters that are chosen such that the contact area with the Si is the same as for the particles in Fig. 1(a). From Fig. 1(b), we can see that while the R1 resonance is mostly unaffected by the small change in diameter, shifts in the R2 resonance wavelength are observed. Reducing the diameter to d-2r blue-shifts R2 by $\Delta\lambda_{R2}$ = 98 nm (particle D), while increasing the diameter to d + 2r red-shifts R2 by $\Delta\lambda_{R2}$ = 91 nm (particle E). Moreover, the shifts due to the change in particle diameter in Fig. 1 (b) are similar to those due to the change in edge shape in Fig. 1(a), for the same contact area. This is because the origin of the shift is the same in each case, due to the nature of the resonant mode. The resonance condition can now be written as $d \pm 2r = {}^{m}/_{2}\lambda_{spp} + l_{\varphi}$, where `-` is for particles A and D and ` + ` is for C and E. Differences in the magnitude of $\Delta\lambda_{R2}$ are attributed to changes in the term due to phase-shift, l_{φ}, introduced due to the different edge shapes.

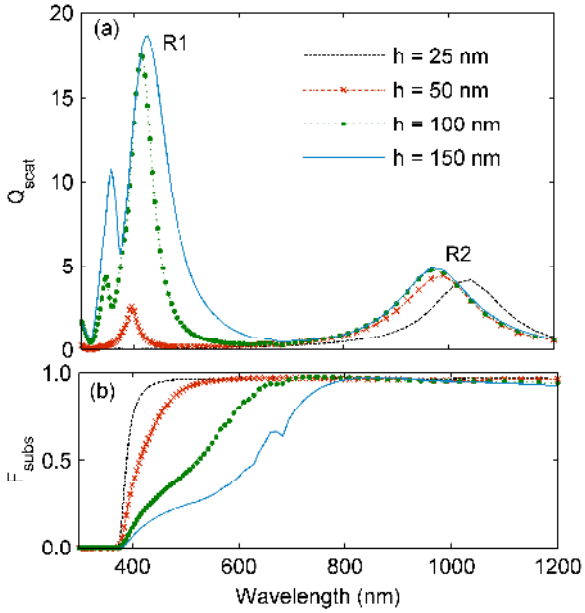

Fig. 2. (a) Calculated normalised scattering cross-section (Q_{scat}), and (b) fraction of scattered light scattered into the Si substrate (F_{subs}) for d = 100 nm, Ag, disk-shaped nanoparticles, directly on a Si substrate, with light incident from air. Data is shown for varying particle height, where h = 25-150 nm.

Figure 2 shows the Q_{scat} and F_{subs} spectra for disk-shaped particles of fixed diameter and varying height. As above, the particles are directly on a Si substrate, with light incident from air. In Fig. 2(b), F_{subs} falls to zero at wavelengths below 400 nm as Si is strongly absorbing at short wavelengths and light scattered into the substrate is absorbed before reaching the surface over which the integration of the scattered power is performed. We can see that increasing the particle height from 50 nm to 150 nm has no effect on either the strength or the position of resonance of the resonant SPP mode R2 (Fig. 2(a)), and that the coupling efficiency at wavelengths corresponding to R2 is unchanged by the increased height of the particles (Fig. 2(b)). This is consistent with the fact that this mode is localised at the interface. However, the strength of the R1 mode increases significantly with particle height, with the largest increase from Q_{scat} = 2.5 for h = 50 nm to Q_{scat} = 17.5 for h = 100 nm, while for very short particles the

#153057 - $15.00 USD Received 19 Aug 2011; revised 19 Sep 2011; accepted 20 Sep 2011; published 23 Nov 2011

R1 mode is entirely suppressed. From Fig. 2(b), it is clear that the increase in strength and broadening of R1 with increasing height, observed in Fig. 2(a), results in reduced coupling efficiency at the corresponding wavelengths.

This has been seen experimentally by Temple who observed a second, local minimum at short wavelengths in transmission spectra for random, self-assembled Ag particles, with d ~60 nm on glass substrates [18]. The strength of the mode increased with increasing particle height, as the particle arrays were annealed.

As the R1 mode is localised at the top of the particle, increasing the particle height is equivalent to moving the resonance away from the substrate. For this reason, we can attribute the dependence of R1 on height to two contributing factors: changes in the electric field driving the resonance and changes in the polarisability of the particle. For front located particles, the driving field is at a minimum at the interface and oscillates with distance from the substrate, due to inference between incident and reflected light. This results in an driving field intensity that is roughly 3 times higher for a resonance 100 nm from the substrate compared to one 50 nm from the substrate. The polarisability of the particle is also affected by the distance to the substrate, which increases with distance from the interface for dipole-like excitations [12], [17]. Additionally, the particle volume, V, is increasing as the height increases. From the quasi-static approximation we would expect the strength of the resonance to increase with volume. For taller particles, with h = 100 nm and 150 nm, an additional mode appears at short wavelengths. These peaks are attributed to higher order free-space modes, although this is not investigated further in this paper.

It is clear that the SPP model allows us to qualitatively predict the scattering behaviour of plasmonic particles on high index substrates as the morphology of the particle is varied. Even small changes in the edge shape can have a significant impact on the resonance wavelength of the mode. Such small variations can result from different nanoparticle fabrication methods, for example, nano-imprinting, followed by a lift-off procedure [21], evaporation and annealing of thin metal films [22,23], and deposition and annealing of colloidal particles [5]. Understanding the sensitivity of the nanoparticle scattering behaviour to small changes in edge shape, which is not predicted by the dipole model, can aid the design of scattering structures and the interpretation of experimental results. The SPP model also demonstrates that nanoparticle height is an important parameter for optimising the in-coupling of light. By reducing the height of the nanoparticles to suppress the R1 mode, we can avoid coupling scattered light out of the cell at short wavelengths, while maintaining strong scattering, and high coupling efficiencies at longer wavelengths.

So far we have not discussed the effect of the *phase* of the scattered light, with respect to the incident light. It has been widely reported that scattering from plasmonic particles can result in a reduction of transmission into the substrate at short wavelengths [21,22,24,25]. This has been attributed to destructive interference between the light scattered and the incident light, due to the large phase component of the polarisabilty of a dipole-like scatterer at wavelengths below resonance [21]. It is important to note that this is a property of *all resonant modes* in a continuum of non-resonant modes, and does not depend on the nature of the resonance [23]. For this reason we should discuss the implications of Fano resonances for resonant SPP modes.

It has been reported that the wavelength region over which suppression in the transmission occurs depends on the particle shape [15], [22], [26] as well as dielectric environment [24], [25], [22]. When located on the front of a solar cell, disk shaped particles capable of supporting resonant SPP type modes demonstrate the most severe suppressions in the wavelength region under discussion (400 to 1000 nm) due to the fact they have red-shifted resonances relative to spheres of the same radius [22]. However, although the amount of light transmitted at the interface is important to consider for anti-reflection effects, it is not always useful when evaluating light trapping for a number of reasons. Firstly, enhancement in transmission does not take into account the light trapping effect, which requires knowledge of the portion of light coupled into trapped modes in the Si [27]. Secondly, we have recently shown experimentally that the light trapping effect can overcome the reduction in

#153057 - $15.00 USD Received 19 Aug 2011; revised 19 Sep 2011; accepted 20 Sep 2011; published 23 Nov 2011

transmission if the suppression occurs in the light trapping region, for particles located on the front of the cell [16]. In other words, although less light is transmitted into the Si due to the presence of the particles, it is scattered at high angles and trapped, and hence will increase the overall absorption if the cell is sufficiently thin. Finally, suppression at short wavelengths can be avoided entirely by locating the particles on the rear of the cell [25], which is the optimal configuration for particles supporting resonant SPP modes as the scattering cross section can be over 3 times larger relative to particles located on the front [17]. For these reasons, we concentrate on rear located particle arrays and we employ a multi-scattering model taking into account the optical losses of the particles to evaluate the light trapping provided by nanoparticles supporting SPP modes.

2.2 Rear located particles

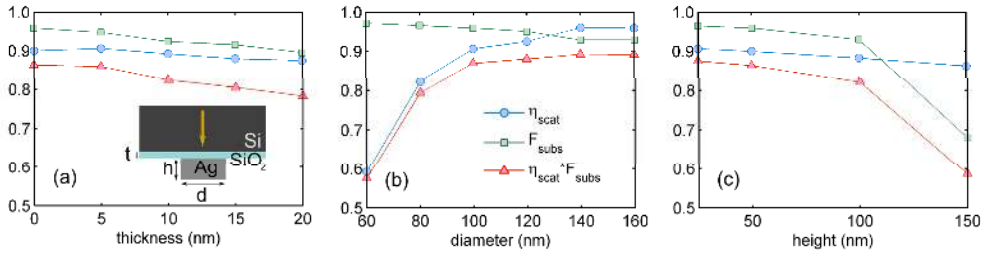

Fig. 3. Average scattering and coupling efficiency calculated over the light trapping spectral region for a 2 μm thick, Si substrate (500 nm to 1200 nm) for rear located particles. For (a) d = 100 nm, h = 50 nm and varying spacer layer thickness from 0 to 20 nm, (b) t = 0 nm, h = 50 nm and varying diameter from 60 to 160 nm, and (c) t = 0 nm, d = 100 nm and varying height from 25 to 150 nm.

Previous work on the scattering behavior of front and rear located, disk-shaped nanoparticles has shown that the spectral position of the resonance peak and the coupling efficiency spectra are the same whether the particles are located on the front or on the rear [14]. For this reason, the design considerations described in section 2(a) hold for rear located particles. Figure 3 shows a summary of the optical losses in Ag nanoparticles, located on the rear of the substrate, as the spacer layer thickness, t, particle diameter, and height are varied. The average scattering and coupling efficiency are calculated over the light trapping spectral region for a 2 μm thick, Si substrate, defined as 500 nm to 1200 nm: from the wavelength at which transmission losses exceed 10%, to the band edge of Si. The trends observed can be qualitatively predicted by the SPP model. Figure 3(a) shows that the average F_{subs} decreases with increasing t as it is well known that the coupling efficiency depends on the overlap between the particle near field and the Si [13], however η_{scat} is not significantly affected as the nature of the excitation at the interface is not changed. In Fig. 3(b), data for particles with diameters from 60 to 160 nm are shown: any larger and the scattering peak is red-shifted beyond the band edge of the Si substrate. The scattering efficiency does not change significantly for larger particles as the diameter is changed, but decreases sharply for d < 100 nm. For these particles, d is significantly smaller than $^{m}/_{2}\ \lambda_{spp}$ and the quasi-static approximation is more appropriate to describe the behaviour of resonant mode [28]. The change in diameter does not affect F_{subs} significantly as the overlap of the near field is the same for all values of d. In Fig. 3(c), the coupling efficiency reduces as the height of the particle increases due to the increasing influence of the R1 mode, however η_{scat} is not significantly affected as the excitation at the interface is insensitive to changes in particle height.

It is clear that to minimise the optical losses for Ag, disk-shaped nanoparticles, the resonant SPP mode (R2) should be excited as close to the semiconductor surface as possible, and that the R1 resonance should be suppressed. To achieve this spacer layers should be avoided or kept to a minimum and the particle geometry should be chosen such that the height is 50 nm or less, and the diameter is in the range between 100 and 160 nm.

#153057 - $15.00 USD Received 19 Aug 2011; revised 19 Sep 2011; accepted 20 Sep 2011; published 23 Nov 2011

3. Evaluation

We will now evaluate a random array of optimal scattering nanoparticles for light trapping. It is difficult to meaningfully compare light trapping for different devices as the factor by which absorption is enhanced depends not only on the efficiency of the light trapping, but also on the thickness of the device, the absorption of the material and the wavelength region under study. Comparing path length enhancements of the light in the material is one way to overcome these difficulties; however this is only useful in the limit of weakly absorbed light. In order to provide a meaningful comparison we compare our plasmonic scattering structures with an ideal Lambertian rear reflector as well as other standard light trapping schemes. Additionally, we would like to calculate the overall absorption enhancement in such a way that the physical effects of losses are elucidated. To do this we employ the formalism introduced by Goetzberger to estimate the light absorbed in a 2 μm Si substrate [29]'[30].

Goetzberger originally described a multi-scattering method of calculating the absorption enhancement provided by a Lambertian-type diffuse reflector on the rear of a finite Si substrate [29]. This method can be generalised for any type of rear scattering surface, as long as the angular distribution of light reflected at the rear interface is known. Additionally, losses can be included by modifying the coefficient for diffuse reflectance at the back surface, R, which determines the fraction of the light back-scattered into the substrate after each scattering event. For an ideal Lambertian surface, R is assumed to be 1; however, for nanoparticles we can include Ohmic losses and out-coupling losses by setting R equal to η_{scat} and F_{subs} respectively. In using the Goetzberger formalism to evaluate light trapping due to plasmonic nanoparticle scattering, we make the following assumptions: 1) that we have an array of identical, randomly positioned particles, that is sufficiently dense to extinguish all light incident at the back surface of the substrate over the light trapping spectral region, and 2) that it is sufficiently sparse that inter-particle interactions are negligible and the scattering behaviour of the array as a whole is simply the aggregate of the scattering behaviour of the single particle case. We will discuss the validity of these assumptions in more detail later.

The angular spectrum of light scattered into the Si by a nanoparticle can be determined from 3D numerical simulations. The Poynting vector of the scattered field was calculated over two orthogonal surfaces bisecting the particle; one parallel, and one perpendicular to the polarisation direction (resulting in P_x, P_z and P_y, P_z components respectively). Since the particles are rotationally symmetric, we can calculate the particle's response to unpolarised light by averaging the P_x and P_y components and the P_z components separately at corresponding points on the planes. The magnitude of the averaged Poynting vector and the direction of propagation relative to the normal was found for a loci of points 500 nm from the particle centre in the Si substrate. This distance was chosen to ensure that the calculation was performed away from the high field gradients of the particle near-field. To good approximation, this is the angular distribution of scattered light, I_{scat}, in the Si substrate, averaged over the 2 possible linear polarisation directions, at a given wavelength. The calculation was repeated for wavelengths from 500 nm to 1200 nm, spanning the light trapping spectral region.

#153057 - $15.00 USD Received 19 Aug 2011; revised 19 Sep 2011; accepted 20 Sep 2011; published 23 Nov 2011

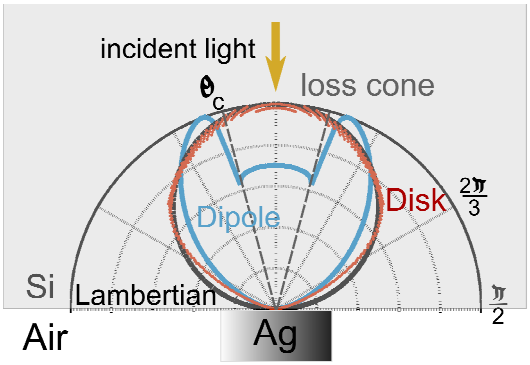

Fig. 4. Calculated angular distribution of light scattered into the substrate (I_{scat}) at the R2 resonance, λ_{R2} = 990 nm. Data is shown for a d = 100 nm, h = 50 nm, disk-shaped nanoparticle (Disk, red), a horizontally orientated dipole (Dipole, blue) and an ideal Lambertian scatterer (Lambertian, black), on the rear of a Si substrate. The loss cone for a Si/Air interface is also shown (dashed line, grey), defined by the critical angle (θ_c).

Figure 4 shows the angular distribution of light scattered into the Si substrate, I_{scat}, by rear-located scattering structures. Data is shown for a 50 nm radius, 50 nm tall disk-shaped, Ag nanoparticle, calculated at the resonance wavelength for the R2 mode, λ_{R2} = 990 nm (Disk, red), and a horizontally oriented dipole located in the air region, directly at the interface with the Si substrate (Dipole, blue). The scattering distribution of the dipole is calculated using the method developed by Mertz [12]. Isotropic scattering from a Lambertian back reflector, calculated as $I_{scat} = \cos(\theta)$ is plotted for comparison (Lambertian, black).

For particles directly on the substrate, the angular distribution at resonance is similar to the Lambertian case, and not the dipole case. We attribute the different angular distributions for the disk and the dipole to the different types of resonant mode excited, since it is known that the angular dependence of scattered light depends strongly on the mode [31]. The fraction of the scattered light that is trapped after each scattering event was calculated by integrating I_{scat} in the Si over the solid angle outside the loss cone, and dividing by the total scattered power. The loss cone for a Si/Air interface is defined by the critical angle, $\theta_c = \arcsin(1/n_{Si})$, as illustrated in Fig. 4 (grey, dashed line). For the nanoparticle shown, 91% of the scattered light is trapped at the R2 resonance. This calculation was repeated for nanoparticle scattering at wavelengths spanning the light trapping spectral region, and the fraction trapped was found to vary by less than 2%. For comparison, 92% of light will be trapped after scattering from an ideal Lambertian surface, and 94% for a dipole directly on the Si surface at a wavelength of 990 nm.

#153057 - $15.00 USD Received 19 Aug 2011; revised 19 Sep 2011; accepted 20 Sep 2011; published 23 Nov 2011

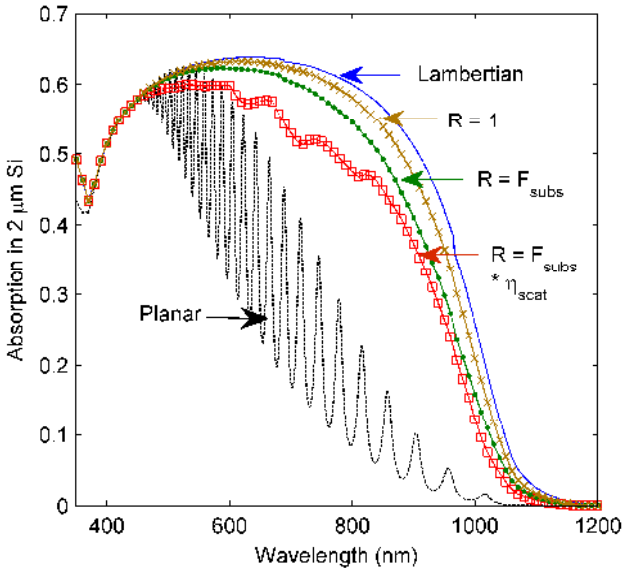

Fig. 5. Calculated absorption in a 2 μm Si substrate, normalised to the incident light intensity. Data is shown for a substrate with planar front and rear surfaces (Planar, dashed line), for a substrate with an ideal Lambertian reflector (Lambertian, solid line), and for rear-located, disk-shaped, Ag nanoparticles, with d = 100 nm and h = 50 nm. The nanoparticles are modelled with no losses (R = 1, brown line), with some fraction of the scattered light coupled out of the cell (R = F_{subs}, green line) and with out-coupling and absorption in the particles (R = F_{subs}*η_{scat}, red line).

Figure 5 shows the calculated absorption in a planar 2 μm Si substrate, with and without light trapping. Absorption spectra are shown for a Lambertian texture (Lambertian, blue solid line) and for an array of Ag nanoparticles at the rear surface. The absorption in a planar 2 μm Si substrate was calculated using the transfer matrix method outlined in ref [32], taking into account reflections from both the front and rear surfaces (Planar, black, dashed lines). Roughly 30% of the light is reflected at the front surface, and the absorption spectrum exhibits interference fringes at wavelengths at which transmission losses occur. After scattering at the rear surface, the light is no longer coherent and therefore the interference fringes disappear for the cases with light trapping. The angular distribution of scattered light for the nanoparticles was taken at the resonance wavelength, as shown in Fig. 4. This simplification was deemed justified as scattering by the particles in the light trapping spectral region is dominated by the R2 mode, as evident from the Q_{scat} spectra of a disk in Fig. 1(a). Additionally, the fraction of light scattered outside the loss cone does not change significantly over the wavelength range of interest. We then compare the light trapping provided by a random array of disk-shaped nanoparticles, located directly on the Si rear surface.

Initially, we assume that scattering from the particles is lossless; that is, all light reaching the back surface is scattered back into the Si with the angular distribution shown in Fig. 4. This is equivalent to assuming a diffuse reflectance equal to 1 at the rear surface. In this case (R = 1, brown line), the enhancement provided by the particles is comparable to the ideal Lambertian case. We then extend the analysis to include the fraction of light that is coupled out of the Si by the particles. This is achieved by setting the diffuse reflectance equal to F_{subs}. The enhancement is then reduced over all wavelengths (R = F_{subs}, green line). Finally, we account for absorption losses in the particles by including the scattering efficiency, defined as $\eta_{scat} = Q_{scat}/(Q_{scat}+Q_{abs})$. Now the enhancement is further reduced over all wavelengths (R = F_{sub}*$\eta_{scat,}$ red line).

#153057 - $15.00 USD Received 19 Aug 2011; revised 19 Sep 2011; accepted 20 Sep 2011; published 23 Nov 2011

Table 1. Enhancement in absorption in a 2 μm Si substrate over the AM1.5g solar spectrum relative to planar case (Λ_{abs}) for different light trapping schemes for given values of reflection from the rear surface (R).

No Optical Losses			With Optical Losses		
Scatterer	**R**	**Λ_{abs} (%)**	**Scatterer**	**R**	**Λ_{abs} (%)**
Lambertian	1	70	Lambertian	$1-1/n_{Si}^2$ (0.93)	58
Dipoles	1	71	Dipoles	F_{subs} (0.98)	66
MNP	1	66	MNP	F_{subs} (0.96)	60
				η_{scat} (0.90)	55
				$F_{subs}*\eta_{scat}$ (0.86)	50

As a figure of merit we calculate the total absorption in the Si over the solar spectrum by convolving the absorption spectra with the incident irradiance per wavelength in the AM1.5g solar spectrum, with the integration carried out over the calculated wavelength range from 350 to 1200 nm. This corresponds to the maximum obtainable photocurrent enhancement. The percentage enhancements in total absorption relative to the planar case, Λ_{abs}, are shown in Table 1 for different light trapping schemes.

The left hand side of Table 1 gives the enhancement values for a Lambertian surface, ideal (non-interacting) dipole scatterers, and an optimised nanoparticle array (MNP), with R set to 1. The differences in Λ_{abs} are entirely due to discrepancies between the angular spectrums shown in Fig. 4, demonstrating the importance of taking into account the propagation direction of the scattered light as well as the total intensity. As the nanoparticles are more forward scattering than ideal dipoles or Lambertian surfaces, they provide lower enhancements, even when losses are neglected.

In the right hand side of the table we introduce optical losses. Firstly, we compare out-coupling losses. For a Lambertian surface, $F_{subs} = 1-(1/n_{Si}^2)$. Now, both MNP and dipole scatterers are more favourable than the Lambertian scatterer. Once again, ideal dipoles directly on the interface show the largest enhancement. We should note however, that the enhancement achieved is dependent on the separation of the dipole from the substrate and raising the dipole moment even 20 nm off the surface will reduce Λ_{abs} to 61%. Additionally, dipole resonances have scattering cross-sections reduced by up to 80% relative to the free space resonance when in close proximity to a Si interface. For nanoparticles taking into account out-coupling only ($R = F_{subs}$), Λ_{abs} is reduced by10% relative to the case with no losses considered (R = 1). This illustrates the fact that light trapping enhancements are very sensitive to small optical losses as they occur at *each* scattering event; significant gains in absorption rely on multiple passes of the cell and hence multiple scattering events. For this reason it is critical that optical losses remain low.

For an array of optimal Ag nanoparticles, taking into account Ohmic losses and out-coupling, the enhancement is 50%, or 71% of the ideal Lambertian case We can compare this to the enhancement due to standard light trapping schemes. From the estimate by Trupke, based on experimental results, pyramids textured into the Si interface result in a path length enhancement of PLE=16 [33]. The absorption in a substrate due to this PLE can be estimated [34]

$$A = \frac{1-R(\lambda)}{\frac{1-R(\lambda)}{PLE\alpha(\lambda)W}+1}, \qquad (1)$$

where W is the width, $\alpha(\lambda)$ is the absorption coefficient, and R is the reflectance of the substrate. This results in Λ_{abs} = 47%, or 67% of the ideal Lambertian case. This result suggests that plasmonic scatterers which support SPP type modes can provide better enhancement than the conventional light trapping used industrially. Here it should be noted that this type of texturing is not applicable for 2 μm thick cells as the pyramid dimensions are on the order of a few microns. For thin cells, randomly rough surfaces are routinely used to

#153057 - $15.00 USD Received 19 Aug 2011; revised 19 Sep 2011; accepted 20 Sep 2011; published 23 Nov 2011

provide light trapping instead. In general, these will have optical losses associated with them too in the form of absorption and non-ideal reflection. Additionally, roughening the surface of the active area can increase surface recombination losses and reduce the semiconductor quality. One of the main benefits of using nanoparticle scattering arrays for light trapping applications is that the particles can be fabricated on thin cells without significantly affecting their electrical performance. Recently published experimental results show that light trapping provided by random Ag nanoparticle arrays on the rear of thin Si solar cells compare favorably with the enhancements due to conventional diffuse rear-reflectors [3].

In the analysis above we have implicitly assumed that the total light scattered by the array is simply the summation of the light scattered by individual particles (and dipoles). We have demonstrated previously that the trends in scattering behavior of relatively dense, random arrays of nanoparticles measured experimentally, can be well represented by averaging the scattering behavior of single particles calculated numerically [25]. These arrays generally have particle surface coverages of around 35%. The rear-located particles under discussion have scattering cross-sections at resonance of around 8 times their cross-sectional area, from ref [17], which is adequate to scatter a large fraction of the light at these particle densities. We have also assumed that all light under goes extinction by the nanoparticles over the whole light trapping spectral region. This requires the array to have broad scattering resonances, which is not necessarily true of an array of identical particles. However, the results from Fig. 1(b) indicate that the wavelength at which resonance occurs can be tuned by changing the diameter. As long as the diameters of the particles are kept above 100 nm, the losses should be minimized as shown in Fig. 3(b). This allows the possibility of designing arrays of disk-shaped particles with varying diameters, which scatter strongly over the whole solar spectrum, and couple well to the substrate. An optimized array could be fabricated by using the soft-stamp nanoimprint lithography technique.

4. Conclusion

We have demonstrated that the resonant SPP conceptual model can be used to qualitatively predict the scattering behaviour of plasmonic nanoparticles on high index substrates. By understanding the nature of the resonant mode, we can predict that scattering from plasmonic particles is sensitive to the area of the particle in contact with the substrate, and that reducing the height of the particles can suppress out-coupling of light at short wavelengths while maintaining strong scattering in the light trapping spectral region. This allows the possibility of designing arrays of disk-shaped particles with varying diameters which scatter strongly over the whole solar spectrum and couple well to the substrate. Taking into account optical losses we estimate that an optimal array of randomly positioned nanoparticles on a 2 μm Si substrate can provide up to 71% of the enhancement in absorption achievable with an ideal Lambertian rear-reflector, compared to an estimate of 67% for conventional pyramid-type light trapping schemes.

Acknowledgments

The research at ANU is financially supported by the Australian Solar Institute, the Australian Research Council and the EU FP7 PRIMA project. The Authors would also like to acknowledge the Australian National University Supercomputer facility for supplying computational resources.

#153057 - $15.00 USD Received 19 Aug 2011; revised 19 Sep 2011; accepted 20 Sep 2011; published 23 Nov 2011